Size and support effects for CO adsorption on gold model catalysts

Sh.K. Shaikhutdinov *, R. Meyer, M. Naschitzki, M. Bäumer, and H.-J. Freund

Department of Chemical Physics, Fritz-Haber-Institut der Max-Plank-Gesellschaft, Faradayweg 4–6, 14195 Berlin, Germany

Received 22 October 2002; accepted 6 December 2002

CO adsorption on gold particles deposited on well-ordered alumina and iron oxide films was studied with temperature-programmed desorption. Scanning tunneling microscopy was used to provide correlative structural characterization. The results show that the adsorption of CO on gold exhibits a size effect in that small particles adsorb CO more strongly. For a given particle size (~3 nm), CO desorption temperature (at ~170 K) is essentially independent of the supports studied. Therefore, support effects seen in CO oxidation on real catalytic systems must arise from the interaction of oxygen rather than CO with these catalysts.

KEY WORDS: gold; nanoparticles; carbon monoxide; CO oxidation; particle size effects; temperature-programmed desorption; scanning tunneling microscopy.

1. Introduction

Gold has long been regarded as an inert surface. However, in the past decade, mainly through the efforts of Haruta and co-workers [1,3], gold nanoparticles have begun to attract attention owing to their unique catalytic properties. In recent years, highly dispersed gold has been shown to be an effective catalyst for many reactions [1–9]. Low-temperature CO oxidation is of particular importance, finding applications in indoor air quality applications [10] and as a guard bed catalyst to prevent CO poisoning of proton exchange membrane fuel cells [11,12].

The catalytic performance of gold in CO oxidation depends critically on the particle size. While particles about 3 nm are generally the most active [13,14], gold clusters of eight atoms deposited on MgO(100) have been shown by Heiz *et al*. also to be active [15]. In addition, Campbell's group found that smaller gold particles supported on TiO_2(110) exhibited stronger adsorption of atomic oxygen [16].

Of particular interest are the role of the support and the origin of any differences in catalytic activity between gold catalysts on non-reducible oxides (*e.g*. Al_2O_3) and reducible oxides (*e.g*. Fe_2O_3) [17]. In order to shed light on the size and support effects in the CO oxidation reaction, it is necessary to study first the individual adsorption of CO and O_2 on small gold particles of controllable size. In this context, gold particles deposited on thin oxide films appear to be suitable model systems, as has been shown previously for other metals and reactions [18–23].

* To whom correspondence should be addressed.
E-mail: shaikhutdinov@fhi-berlin.mpg.de

CO adsorption on gold has previously been studied on several single crystalline surfaces. Outka and Madix [24] observed CO_2 formation from reaction of atomic oxygen (formed by an atomic oxygen source) with CO on Au(110), but CO was found not to adsorb on the gold surface at temperatures above 125 K. Ruggiero and Hollins [25] studied the adsorption of CO on a stepped Au(332) surface. Although CO was observed to desorb in two peaks, at 140 and 185 K, infrared spectroscopy was unable to resolve these states in a definitive manner. Density functional theory calculations by Nørskov's group [26] strongly indicate that CO may only chemisorb on the low-coordinated Au atoms such as steps and kinks, and not on the regular (111) terraces.

In the present work, we focused on CO adsorption on Au nanoparticles formed on well-ordered alumina and iron oxide (FeO, Fe_3O_4) films. The structures of these supports have already been studied in previous work [21–23,27–30].

2. Experimental

The experiments were performed in two separate ultra-high-vacuum chambers: the first was used primarily for temperature-programmed desorption (TPD) experiments using a differentially pumped quadrupole mass spectrometer (QMS) (Fisons), while characterization by scanning tunneling microscopy (STM) (Omicron) was performed in the second chamber. Both chambers were equipped with an Auger electron spectroscopy/low-energy electron diffraction (AES/LEED) instrument. For metal (Fe 99.99%, Au 99.99%, Goodfellows) deposition, we used electron beam-assisted metal evaporators (Focus EFM3). Note that, during evaporation, a retarding

1011-372X/03/0300-0211/0 © 2003 Plenum Publishing Corporation

potential was applied to the sample to avoid any sputtering caused by acceleration of the metal ions toward the sample.

Gas (CO 5.0 and O_2 5.0, AGA Gas) exposures for both oxide film preparation and adsorption experiments were performed with a directional doser. For TPD measurements, the sample was placed about 0.5 mm in front of the spectrometer shield with a 6 mm aperture and heated at a rate of 5 K/s.

Thin alumina films were grown on an NiAl(110) single crystal by two cycles of oxidation at 550 K and annealing at 1150 K [21–23,31].

Thin iron oxide films were prepared on a Pt(111) single crystal as described previously [29,30]. Briefly, an FeO(111) overlayer is formed by evaporating ~1 ml of iron on to a Pt(111) single crystal at 300 K and subsequent oxidation at $\sim 10^{-6}$ mbar of O_2 at 1000 K for 2 min. The surface exhibits a characteristic LEED pattern corresponding to a moiré pattern formed by slight rotation of the FeO(111) layer with respect to Pt(111) [27]. The Fe_3O_4(111) films were grown by repeated cycles of iron deposition at 90 or 300 K and subsequent oxidation at ~900 K. The samples were finally oxidized at 10^{-6} mbar of O_2 at 1000 K for 5 min. The quality of the films was judged by LEED.

Gold was deposited at a rate of ~0.1 Å/min as calibrated by a quartz microbalance (sample surface temperatures are noted in the text). For each Au sample, new films were grown.

3. Results and discussion

3.1. Gold on alumina

The clean alumina film has been studied intensively in previous work [21–23,31]. Briefly, the surface exhibits large terraces, on which line and point defects exist, which can act as nucleation centers for metal deposits.

Figure 1(a) shows an STM image of gold (nominal thickness: 0.15 Å) deposited on the alumina film at 300 K. Gold particles, imaged as bright protrusions,

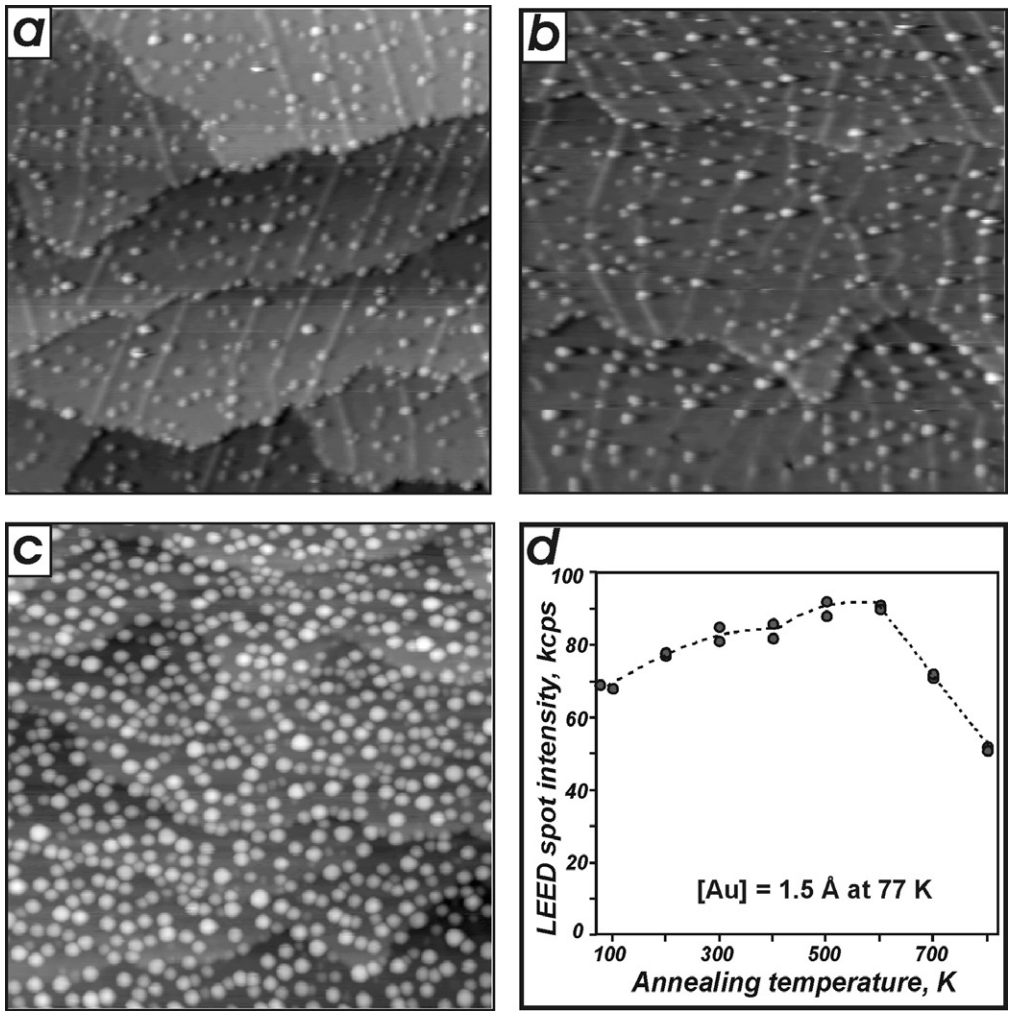

Figure 1. STM images of gold overlayer (nominal thickness: 0.15 Å) on Al_2O_3/NiAl(110) film (a) as deposited at 300 K and (b) annealed to 600 K. (c) STM image for 1.5 Å thick layer after annealing to 600 K. (All images are $100 \times 100\,nm^2$.) (d) Intensity of the LEED spots as a function of annealing temperature for the 1.5 Å thick Au overlayer deposited at 77 K (measurements were performed at 77 K.)

are found on flat terraces as well as on steps and line defects of the oxide layer (see protruding lines across terraces). Based on our previous studies on metal nucleation and growth on alumina film [22], the absence of preferential nucleation indicates that the gold atoms have a fairly low mobility on the alumina surface at 300 K. This result was also observed by Winkler *et al.* [32] in their examination of gold on alumina.

The Au particles exhibit a narrow size distribution centered around 2.5 nm in diameter as measured by STM. Most of the particles are $\sim 0.5 \pm 0.05$ nm high, which corresponds to two layers of Au on the alumina surface. Therefore, the STM images clearly show the formation of very small gold particles on the alumina support. It should also be noted that, owing to the tip-sample convolution effect, STM typically leads to an overestimation of the particle lateral dimensions (but not of their height) by a factor of 2.5–1.5 for the 2–6 nm particles, respectively [33]. For the purposes of this paper, we report the sizes as measured.

The system morphology is found to be fairly stable toward heating up to 600 K [*cf.* images (a) and (b) in figure 1). However, the particle density decreases while the particle size slightly increases to ~3.0 nm in diameter and 0.9 nm in height. Obviously, this can be explained by gold sintering.

The sintering effect is also manifested in the LEED patterns. The intensity of the diffraction spots for the sample after 1.5 Å of gold has been deposited at 77 K gradually increases upon heating from 77 to 600 K [see figure 1(d)] owing to the increasing fraction of the bare oxide surface. At temperatures above 600 K, diffraction strongly attenuates, probably owing to metal diffusion into the thin oxide film as observed before for other metals [34].

The particle geometry was preserved for larger gold depositions. For the 1.5 Å thick gold layer, the average diameter and height were found to be about 4 and 1 nm, respectively [see figure 1(c)]. Therefore the size of the Au particles can be increased in a controllable way by depositing varying amounts of gold, making it possible to study size effects on reactivity of the gold particles.

CO adsorbed at 77 K on Au particles apparently exhibits first-order desorption kinetics for a well-resolved peak at around 180 K, as revealed by the TPD spectra shown in figure 2(a) (note that CO does not adsorb on the alumina film above 77 K). With increasing CO exposure another state emerges at ~120 K. In principle, the two desorption peaks may be assigned to adsorption on the metal and at the metal–oxide interface as suggested for propene adsorption on Au/TiO_2 [35]. Many researchers have speculated about special sites for adsorption at the metal–support periphery ([35—37] and references therein). However, two CO peaks arising from the Au particles are also consistent with the TPD results observed on the stepped Au(332)

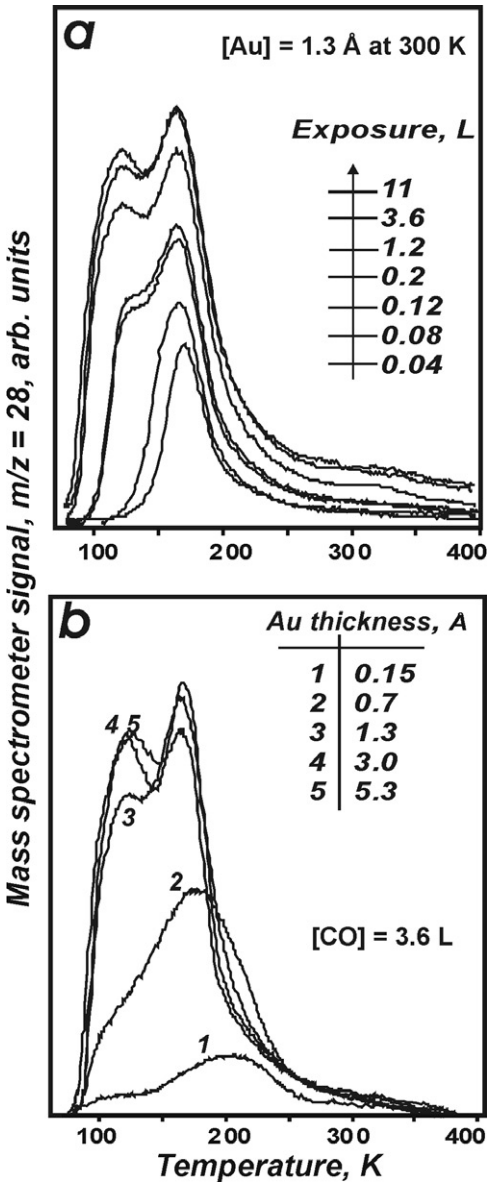

Figure 2. CO TPD spectra for gold deposited at 300 K on $Al_2O_3/NiAl(110)$ as a function of (a) CO exposure and (b) Au coverage. 1 L = 10^{-6} Torr/s.

surface [25]. Therefore, we tentatively assigned both peaks to desorption from gold particles; however, the origin of our low-temperature state is unclear as the desorption starts immediately with heating at saturation exposure.

The position of the high-temperature peak is sensitive to Au coverage. It gradually shifts from 210 to 160 K as the nominal Au thickness increases from 0.1 to 1.3 Å [see figure 2(b)]. This result indicates a particle size effect with respect to CO adsorption: small Au particles adsorb CO more strongly.

The integral intensity of CO desorption signal reaches saturation with further increase in Au coverage as the spectra are nearly identical for the samples possessing 1.3 and 5.3 Å thick Au overlayers. Since theoretical calculations [26] predict that CO only adsorbs on

low-coordinated Au atoms and not on the regular terraces, it seems likely that gold deposition beyond 1–2 Å only leads to the gradual development of the flat terraces which are essentially inert toward CO.

3.2. Gold on iron oxides

3.2.1. Au/FeO(111)

STM study of the clean FeO surface revealed wide, flat terraces separated by monoatomic steps of ~2.3 Å in height characteristic for the Pt(111) substrate underneath the film. The terraces show a honeycomb superstructure with ~30 Å periodicity (moiré pattern) in turn exhibiting an atomic structure with a ~3 Å periodicity [for example, see the inset in figure 3(b)].

Gold deposition at 120 K (and subsequent warming to 300 K for STM measurements) first results in decoration of substrate steps and defects (“holes” in oxide film) as resolved by STM at very low Au coverage [see figure 3(a)]. At increasing coverage, small Au clusters of different sizes also start to nucleate at the terraces [figure 3(b)]. Gold particles grow with further increase in the amount of gold deposited [figure 3(c)], and at high coverage Au

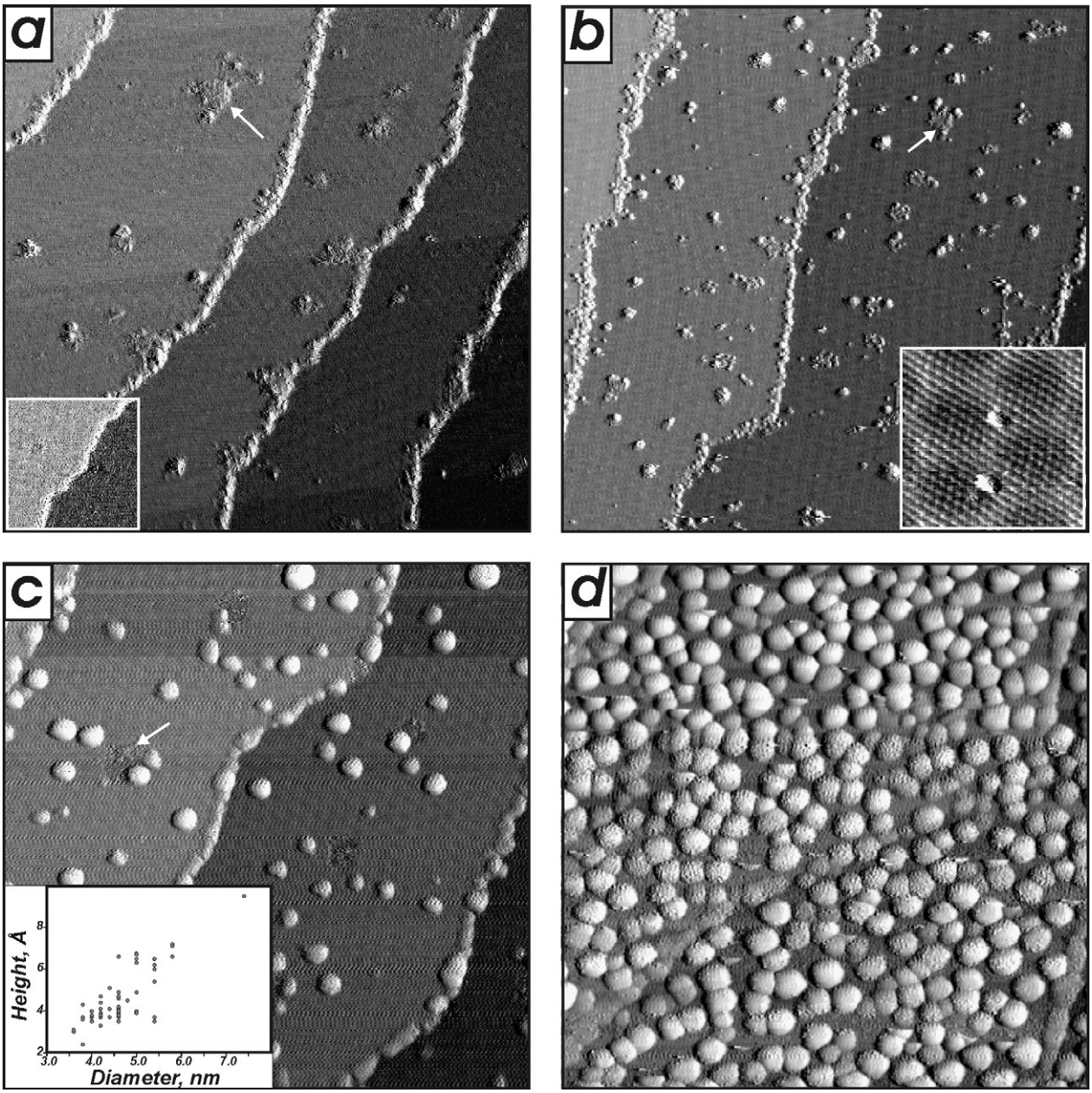

Figure 3. (a) 100 × 100 nm^2 STM images of gold particles deposited on an FeO(111)/Pt(111) film at 120 K at (a) 0.01, (b) 0.05, (c) 0.2, and (d) 2 Å coverage. The images are presented with differentiated contrast. White arrows mark defects (“holes”) of the oxide film. The inset in (a) shows step edges on the clean FeO(111) surface, for comparison. The inset in (b) shows the moiré pattern characteristic for FeO overlayer on Pt(111) with two small Au clusters deposited. The inset in (c) presents the size distribution of the particles imaged in (c), which show that growing particles keep their aspect ratio.

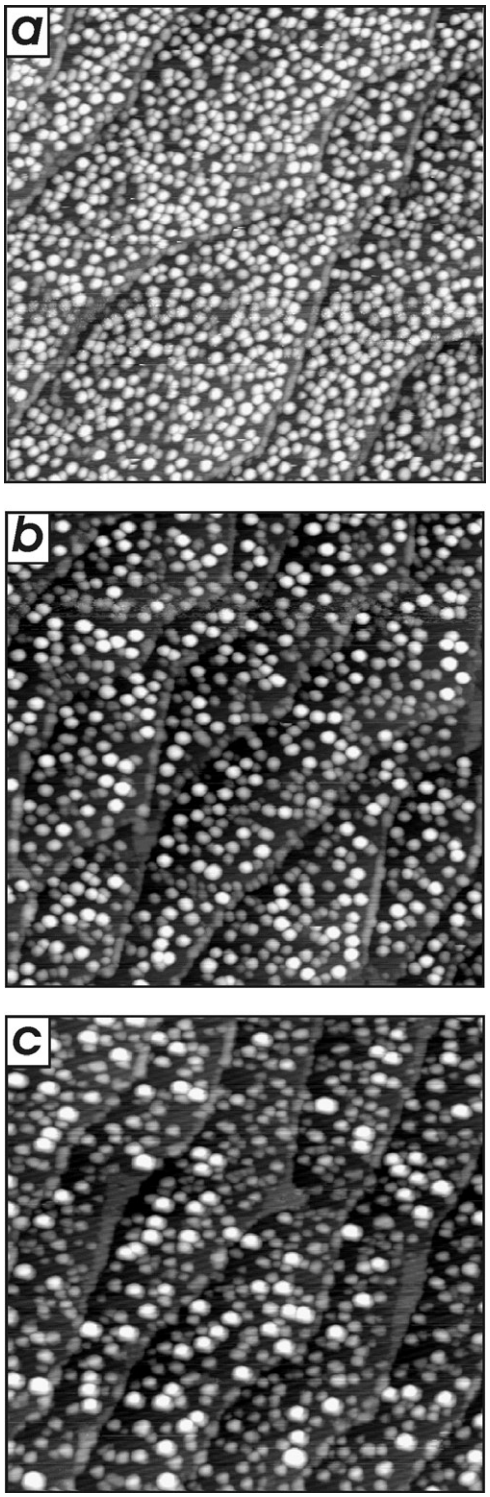

Figure 4. (a) 200×200 nm STM images of 2 Å thick gold overlayer deposited on FeO at 120 K and heated to (a) 300, (b) 500 and (c) 600 K. The particle density decreases and particles apparently become larger at elevated temperatures. In addition, steps become decorated by monolayer gold islands running along the steps.

particles are essentially homogeneously distributed on the FeO surface [figure 3(d)].

On average, the particle size increases with increasing Au coverage and reaches ~5 nm in diameter for a 2 Å thick layer. The aspect (height/diameter) ratio for the particles imaged in figure 3(c) is ~0.1, with a thickness of 2–4 atomic layers. Bearing in mind a tip convolution effect factor of 2, this suggests the real aspect ratio to be ~0.2 and hence the Au particles appear as elongated hemispheres.

Annealing to 500 K does not affect the Au/FeO morphology at low Au coverages (*e.g.*, below 0.2 Å) where the particles are located relatively far from each other. However, at high coverages, some changes upon annealing do occur, as shown in figure 4. Again, as in the case of Au on alumina film, gold sinters upon heating: the particle density decreases while the mean particle size increases. Interestingly, step edges only exhibit gold features one monolayer in height, whereas particles are much higher on the terraces. Upon annealing to 600 K, these gold particles sinter more intensively, thus forming extended monolayer islands running along the step edges, as shown in figure 4(c).

CO TPD spectra for the Au/FeO samples are shown in figure 5 as a function of Au coverage [note that clean FeO(111) film is inert toward CO exposure above 77 K]. The spectra are presented in two panels: (a) the spectra for the samples as prepared by gold deposition at 77 K and (b) those for the same samples annealed to 500 K.

Figure 5(a) shows that, as the gold coverage increases, the CO desorption temperature decreases in line with the particle size effect observed for the above Au/Al_2O_3 system. It seems likely that, when small amounts of gold are deposited at 77 K, small gold clusters are formed owing to the low diffusivity of Au ad-atoms at

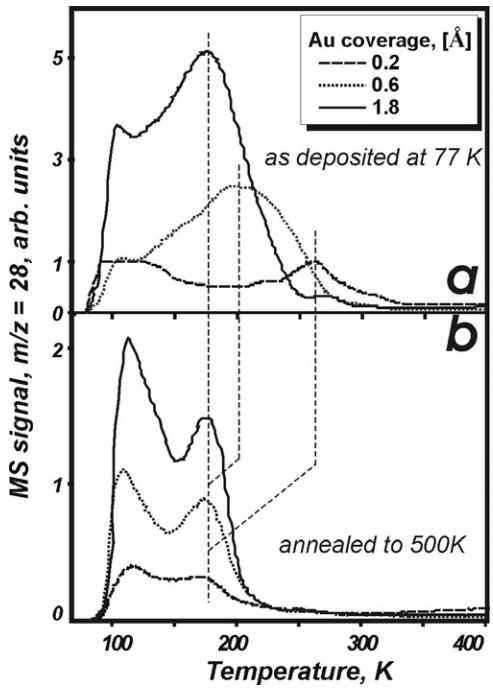

Figure 5. CO TPD spectra for (a) as-deposited and (b) annealed to 500 K gold particles on a FeO(111) film at different Au coverages.

low temperatures. The CO adsorption on these clusters is relatively strong as they mostly consist of low-coordinated Au atoms. Increasing Au coverage favors the formation of larger particles, which adsorb CO less strongly.

However, after annealing the particles to 400 K, we observe three distinct phenomena. First, for a given Au coverage, annealing results in a substantial decrease in the integral CO desorption intensity. Second, the desorption peak shifts to lower temperatures for the annealed samples, with the shift being larger at a low Au coverage. Third, for the annealed samples, the desorption temperature (~170 K) is independent of the Au coverages studied (0.2–1.8 Å).

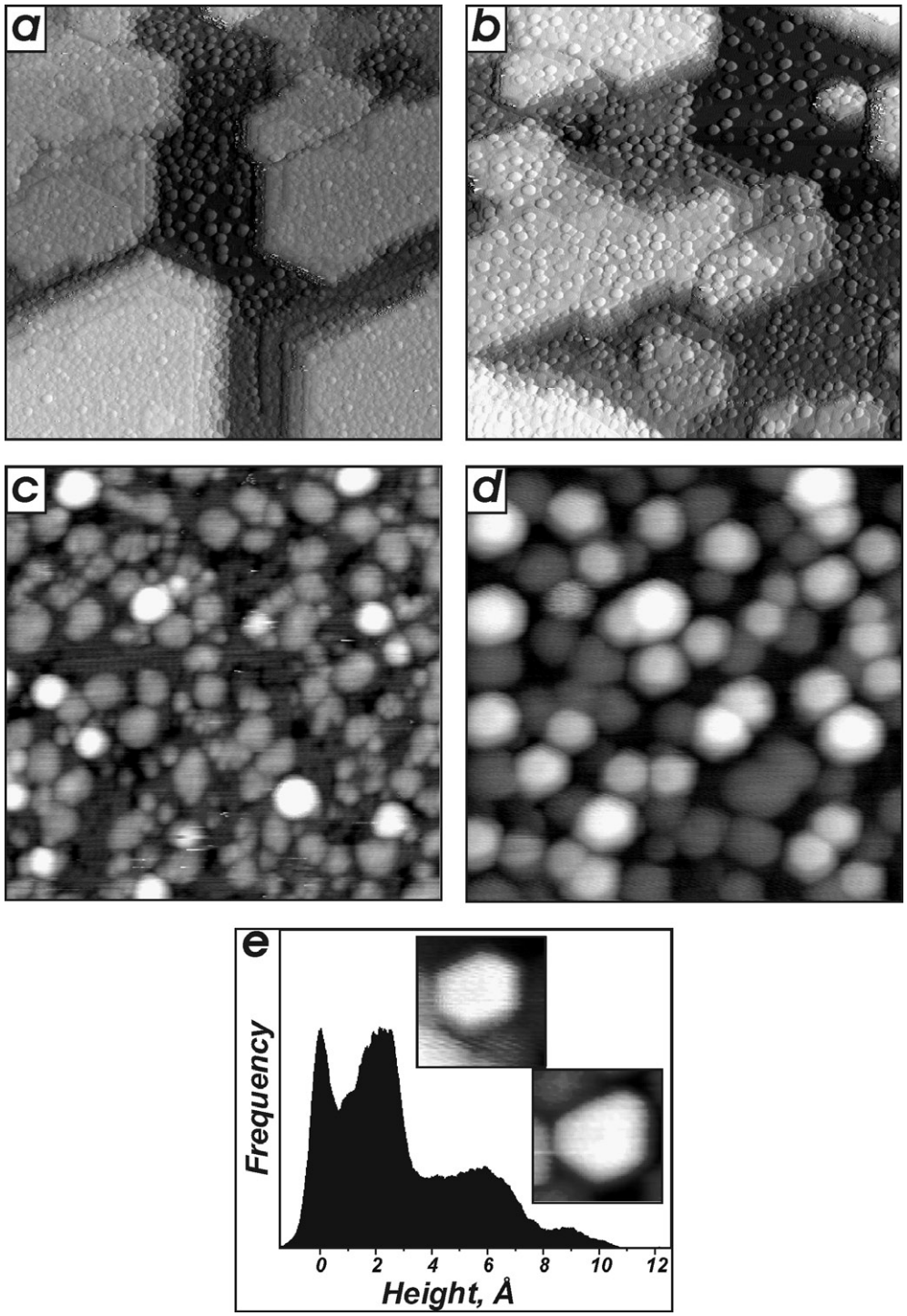

Figure 6. Room temperature STM images of 1 Å thick gold overlayer deposited on $Fe_3O_4(111)$ film at 120 K (a, c) before and (b, d) after annealing to 500 K. Image sizes: (a, b) 200 × 200 nm and (c, d) 40 × 40 nm. Images (a) and (b) are presented with differentiated contrast. The height histogram of particles observed in image (d) is shown in (e) together with the two 7 × 7 nm STM images of the well-faceted Au particles. The histogram clearly shows that particle height is quantized.

These effects can be explained in terms of sintering of the gold deposits upon heating, thus forming larger particles and hence decreasing the total surface area. In addition, particle restructuring may be occurring simultaneous with annealing, resulting in a loss of the low-coordinated Au atoms. The absence of the size effect in the CO TPD spectra for the annealed samples over the coverage range studied [0.2–1.8 Å, see figure 5(b)] may indicate that the effect vanishes as the particles exceed some critical size. Based on the STM images presented in figures 3(c) and (d), this size is probably about 4 nm.

A histogram analysis of annealed particles shows that they exhibit a nearly identical aspect ratio [see also the inset in figure 3(c)] or, in other words, a similar particle shape independent of size. Also, the particle density increases at higher Au coverage, without significant changes in particle size [*cf*. figures 3(c) and (d)]. This leads to the scaling of the number of sites adsorbing CO as a function of Au coverage, as actually observed in spectra (b) in figure 5.

3.2.2. $Au/Fe_3O_4(111)$

Previous STM and LEED studies of the $Fe_3O_4(111)$ films formed on Pt(111) have shown that the regular surface is terminated by one-quarter of a monolayer (with respect to the oxygen sub-layer) of Fe^{2+} cations [27–30]. In addition to terrace steps, the defect structure, which may influence the nucleation and growth of Au particles, includes iron vacancies and, in some cases, small domains exhibiting "biphase ordering" [30].

Figures 6(a) and (c) show room temperature STM images obtained for an ~1 Å thick Au overlayer deposited on the $Fe_3O_4(111)$ film at 120 K. Gold particles are randomly found on the support, which typically exhibits hexagonally shaped terraces separated by monoatomic and multiple steps up to 5 nm as high.

Figure 6(c) clearly shows that Au particles exhibit a relatively broad size distribution at 300 K as compared with the Au/FeO and Au/Al_2O_3 systems studied above. The sizes vary from <1 nm to >4 nm in diameter. It seems likely that gold diffusion on $Fe_3O_4(111)$ is rather limited, thus preventing sintering at 300 K. However, heating to higher temperatures definitely promotes sintering. Indeed, figures 6(b) and (d) show that particles annealed to 500 K appear larger, basically at the expense of small particles originally presented in figure 6(c).

Interestingly, the height histogram of image (d) reveals that the height of the particles is quantized as shown in figure 6(e). This implies that particles grow by increasing the number of shells in the cluster. In addition, the annealed particles are well ordered, exhibiting mostly hexagonal (and trigonal) shape [see images in figure 6(e)]. Therefore, it is possible that the particles are well faceted such that the top surface exhibits the Au(111) face, which matches well with the (111) surface of the oxide. Such an epitaxial relationship between metal and support has been shown by STM for Pd/Al_2O_3 [38] and Pd/FeO [39].

The CO TPD study of Au/Fe_3O_4 turned out to be more complicated than that of FeO and alumina films because the Fe_3O_4 surface may also adsorb CO, which desorbs within the same temperature range as Au surfaces. Several desorption states were observed in CO TPD spectra for the clean Fe_3O_4 films: at *ca*. 120 and 180 K, and a high temperature shoulder at ~220 K [40]. The presence of the high-temperature state depends on the film preparation. It appears that oxidation and annealing steps during film preparation may influence the defect structure of the film. Therefore, this issue needs further investigation.

In order to discriminate CO desorption from gold and support, we subtracted the signals from the clean support as measured prior to gold deposition. The difference spectra are shown in figure 7 as a function of Au coverage. The spectra are presented for (a) the samples prepared by deposition at 77 K and (b) those annealed to 400 K.

For as-deposited Au/Fe_3O_4 samples, the CO adsorption properties are found to be essentially identical with those observed for Au/FeO system [*cf*. figures 7(a) and 5(a)]. The CO TPD spectra exhibit the "typical" size effect, *i.e*., the smaller the particles, the stronger is the CO–Au interaction, with CO desorbing at temperatures as high as 250 K for the smallest Au coverage. This effect seems to be retained at least partly after annealing the Au/Fe_3O_4 surface to 400 K. However, a strong decrease in the CO desorption signal clearly

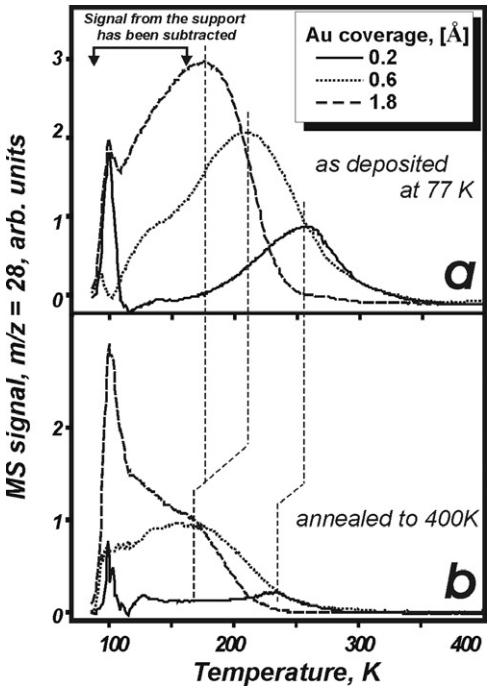

Figure 7. CO TPD spectra for (a) as-deposited and (b) annealed to 500 K gold particles on the $Fe_3O_4(111)$ film at different Au coverages.

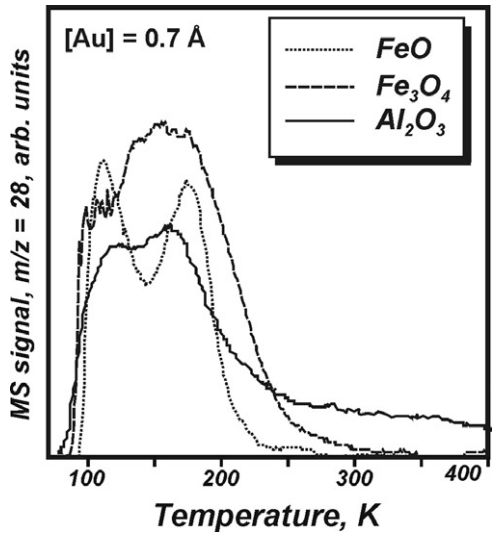

Figure 8. Comparison of CO TPD spectra for gold particles deposited at 77 K and subsequently annealed to 400–500 K for the different supports studied.

indicates the morphology changes upon heating in that particles become larger and more ordered (see figure 6).

In summary, the TPD results observed for Au deposited on Al_2O_3, FeO and Fe_3O_4 films clearly show the particle size effect in that small particles adsorb CO more strongly. It is noteworthy that, for the smallest Au coverage, CO may desorb at temperatures close to 300 K, which is in the temperature range of the working Au catalysts for low-temperature CO oxidation [36]. Note also that such a desorption state has never been observed for Au single crystals.

The size effect is most clearly observed for gold deposited at 77 K. The effect vanishes upon heating to 400–500 K for iron oxide supports owing to sintering effects. It appears that the thermal stability of the smallest Au particles toward sintering depends on the support surface structure and is rather limited on the FeO compared with the Al_2O_3 or Fe_3O_4 surface.

Finally, it is interesting to compare CO TPD spectra obtained at the same (~0.7 Å) Au coverage for various supports. Figure 8 clearly indicates that, for a given particle size (~3 nm), CO interaction with gold particles on different supports is essentially identical.

4. Conclusions

The adsorption of CO on gold has been found to exhibit a particle size effect. Small particles adsorb CO more strongly. The CO interaction with gold model catalysts on various supports is remarkably similar and therefore support effects seen in CO oxidation on real catalytic systems must arise from the interaction of oxygen rather than CO with these catalysts. In addition, the nature of the support and its defect structure may be important for the formation and stabilization of very small Au particles.

Acknowledgments

Financial support from the Deutsche Forschungsgemeinschaft (DFG), Bundesministerium für Bildung und Forschung (BMBF), Fonds der Chemischen Industrie, and EU Network project "Catalysis by Gold" (AURICAT) is gratefully acknowledged. R.M. thanks the Alexander von Humboldt Foundation for a fellowship.

References

[1] M. Haruta, Catal. Today 36 (1997) 153.
[2] G.C. Bond and D.T. Thompson, Catal. Rev. Sci. Eng. 41 (1999) 319.
[3] M. Haruta, and M. Date, Appl. Catal. A 222 (2001) 427.
[4] M. Haruta, N. Yamada, T. Kobayashi and S. Iijima, J. Catal. 115 (1989) 301.
[5] T. Hayashi, K. Tanaka and M. Haruta, J. Catal. 178 (1998) 566.
[6] H. Sakurai, A. Ueda, T. Kobayashi and M. Haruta, J. Chem. Soc. Chem. Commun. (1997) 271.
[7] H. Sakuri and M. Haruta, Catal. Today 29 (1996) 361.
[8] A. Ueda and M. Haruta, Gold Bull. 32 (1999) 3.
[9] T. Aida, R. Higuchi and H. Niiyama, Chem. Lett. (1990) 2247.
[10] G. Srinivas, J. Wright, C.S. Bai and R. Cook, Stud. Surf. Sci. Catal. 101 (1996) 427.
[11] M.M. Schubert, M.J. Kahlich, H.A. Gasteiger and R.J. Behm, J. Power Sources 84 (1999) 175.
[12] S. Thomas and M. Zalbowitz, *Fuel Cells—Green Power* (Los Alamos National Laboratory, 1999).
[13] M. Haruta, S. Tsubota, T. Kobayashi, H. Kageyama, M.J. Genet and B. Delmon, J. Catal. 144 (1993) 175.
[14] M. Valden, X. Lai and D.W. Goodman, Science 281 (1998) 1647.
[15] U. Heiz, A. Sanchez, S. Abbet and W.-D. Schneider, J. Eur. Phys. D9 (1999) 35.
[16] V.A. Bondzie, S.C. Parker and C.T. Campbell, J. Vac. Sci. Technol. A 17 (1999) 1717
[17] M.M. Schubert, S. Hackenberg, A.C. van Veen, M. Muhler, V. Plzak and R.J. Behm, J. Catal. 197 (2001) 113.
[18] D.W. Goodman, J. Phys. Chem. 100 (1996) 13090.
[19] C.T. Campbell, Surf. Sci. Rep. 27 (1997) 1.
[20] C.R. Henry, Surf. Sci. Rep. 31 (1998) 231.
[21] H.-J. Freund, M. Bäumer and H. Kuhlenbeck, Adv. Catal. 45 (2000) 333.
[22] M. Bäumer and H.-J. Freund, Prog. Surf. Sci. 61 (1999) 127.
[23] H.-J. Freund, Surf. Sci. 500 (2002) 271.
[24] D.A. Outka and R.J. Madix, Surf. Sci. 179 (1987) 351.
[25] C. Ruggiero and P. Hollins, J. Chem. Soc., Faraday Trans. 92 (1996) 4829.
[26] M. Mavrikakis, P. Stoltze and J. Nørskov, Catal. Lett. 64 (2000) 10.
[27] W. Weiss, Surf. Sci. 377–379 (1997) 943.
[28] M. Ritter, W. Ranke and W. Weiss, Phys. Rev. B 57 (1998) 7240.
[29] W. Weiss and M. Ritter, Phys. Rev. B 59 (1999) 5201.
[30] Sh. Shaikhutdinov, M. Ritter, X.-G. Wang, H. Over and W. Weiss, Phys. Rev. B 60 (1999) 11062.
[31] R.M. Jaeger, H. Kuhlenbeck, H.J. Freund, M. Wuttig, W. Hoffman, R. Franchy and H. Ibach, Surf. Sci. 259 (1991) 235.
[32] C. Winkler, A. Carew, R. Raval, J. Ledieu and R. McGrath, Surf. Rev. Lett. 8 (2001) 693.
[33] S. Stempel, PhD Thesis, Frei Universität, Berlin, 1998.

[34] M. Heemeier, S. Stempel, Sh.K. Shaikhutdinov, J. Libuda, M. Bäumer, R.J. Oldman, S.D. Jackson and H.-J. Freund, Surf. Sci. (2002) in press.
[35] H.M. Ajo, V.A. Bondzie and C.T. Campbell, Catal. Lett. 78 (2002) 359.
[36] M. Haruta, CATTECH 6 (2002) 102.
[37] L. Guczi, D. Horwath, Z. Pasti and G. Peto, Catal. Today 72 (2002) 101.
[38] K. Højrup Hansen, T. Worren, S. Stempel, E. Laegsgaard, M. Bäumer, H.-J. Freund, F. Besenbacher and I. Stensgaard, Phys. Rev. Lett. 83 (1999) 4120.
[39] Sh.K. Shaikhutdinov, R. Meyer, M. Bäumer and H.-J. Freund, in preparation.
[40] C. Lemire, R. Meyer, H. Kuhlenbeck, Sh.K. Shaikhutdinov and H.-J. Freund, in preparation.